Crown Plaza, Gold Coast, Australia
2-7 December 2007

Application of Pressure-Sensitive Paints to Unsteady and High-Speed Flows

H. Zare-Behtash[1], N. Gongora[1], C. Lada[1] and K. Kontis[1]

[1]School of Mechanical, Aerospace and Civil Engineering
The University of Manchester, Manchester, M60 1QD UK

Abstract

The Pressure-Sensitive Paint (PSP) technique allows the global pressure mapping of surfaces under aerodynamic conditions. The present study involves the application of Tris-Bathophenanthroline Ruthenium Perchlorate based PSP, developed in-house, to two different cases; a) the flow through a sonic nozzle, and b) the examination of the effect of dimples on glancing shock wave turbulent boundary layer interactions at transonic speeds.

Introduction

The process of flow visualisation is of tremendous value in the field of fluid dynamics research. Each technique has certain advantages and disadvantages. In some cases the researcher has economical and spatial limitation whereas in other cases the limitation might be due to the technique itself, for example achieving only qualitative data and a complementary technique is required to achieve better insight into the flow physics.

The current standard for pressure measurement is an array of pressure taps. Pipes connect these holes to pressure transducers, which transform the mechanical force of the pressure to a digital or analog reading. Depending on the size and complexity of the model, the process of creating these models is time-consuming and expensive. Thus the cost (both in terms of time and money) is the first drawback of using a pressure tap system. The second drawback of pressure taps is that they must be limited in number. Drilling small taps into models changes the local pressure distribution at that point, compared to the surface without a hole. Consequently, each tap drilled affects the total pressure distribution, ultimately leading to unrealistic results if too many taps are used. The limitation is in direct conflict with the need for a continuous image of the pressure distribution.

Pressure-sensitive paint (PSP) has become a useful tool to augment conventional pressure taps in measuring the surface pressure distribution of aerodynamic components [8, 2, 7]. PSP offers the advantage of non-intrusive global mapping of the surface pressure. The PSP consists of a dispersion of luminescent probe molecules in an oxygen permeable binder layer. An excitation light source of wavelength λ_e and intensity I_e is used to promote molecules to an excited energy state [4, 10].

An increase in pressure causes a corresponding increase in the partial pressure of oxygen and an increase in the oxygen concentration within the binder layer. This results in a larger level of oxygen quenching and lower luminescence intensity [11]. Because the amount of oxygen in the test gas can be related to static pressures, one can obtain pressure signals from the change in the luminescent intensity of PSP. The relationship between the oxygen concentration and the pressure may be approximated by a second order polynomial [4] , as shown in equation (1).

$$\frac{I_{ref}}{I} = A(T) + B(T)\left(\frac{P}{P_{ref}}\right) + C(T)\left(\frac{P}{P_{ref}}\right)^2 \qquad (1)$$

I_{ref} is the luminescent intensity at a known constant reference pressure, P_{ref}, under wind-off conditions. Coefficients $A(T)$, $B(T)$ and $C(T)$ can be determined by static calibration tests. These coefficients are unique for each temperature.

Experimental Setup

Sonic Nozzle

The pressure field on the sidewall of the complex geometry shown in figure 1 has been examined. The PSP was applied onto the side wall of the test section with the other side covered with optical quality perspex. Before the PSP was applied a layer of white primer was first applied to the model surface as a base coat to eradicate any surface non-uniformities. The model is divided into three main sections with the flow going from right to left. It is comprised of a concave section, an area of constant cross-section and a region bounded by solid straight walls on the top and bottom surfaces, with the inlet pressure varying in the range $1-3$ *bar*. Pressure tappings were placed along the side wall to provide a comparison between the pressures obtained from the transducers and those of the PSP technique.

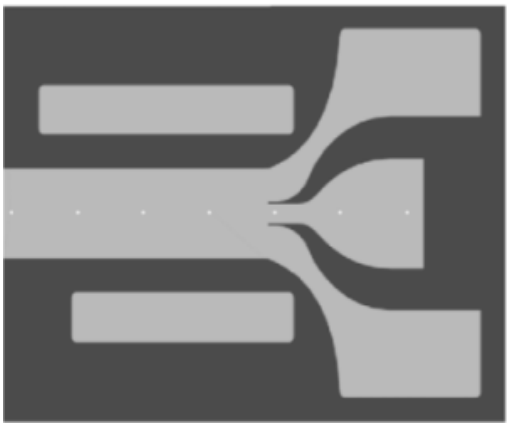

Figure 1: Sonic nozzle under investigation.

Transonic wind tunnel

The control effectiveness of dimples on the glancing shock wave turbulent boundary layer interaction produced by a series of hemi-cylindrically blunted fins at Mach 0.8, was studied in a transonic wind tunnel [5].

The experiments were performed in a closed-return supersonic wind tunnel facility with a rectangular cross section area measuring 100×25 *mm*, at Mach number $M = 0.8$ and Reynolds number $Re = 4.962 \times 10^5$. All models incorporated a hemi-cylindrical leading edge. A series of 2 *mm* diameter, 1 *mm* deep and 3 *mm* spaced dimples were drilled across the hemi-cylindrical leading edge at angles: 0^o, 45^o and 90^o relative to the tip of the leading edge. The schematic diagram of the fins with dimples located at 0^o and 90^o is shown in figure 2. The model blockage ratio was 8%.

Discrete pressure measurements along the side wall of the wind tunnel section were carried out to analyse the validity of the PSP results.

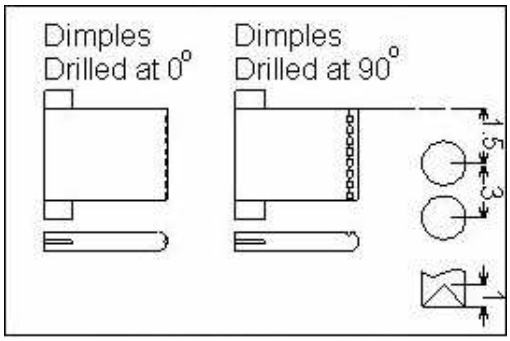

Figure 2: Schematic of the shock generator hemi-cylindrical blunt fins with dimples at 0^o and 90^o.

Results and Discussion

Calibration

For the steady flow through the sonic nozzle, in-situ calibration was applied. Whereas a-priori calibration was applied to the wind tunnel experiments. To obtain a good curve fit between intensity and pressure, a series of data points is required. Because of the inherently unsteady nature of the flow within the wind tunnel, it would not be possible to obtain many pressure readings, and if a polynomial were to be fit to these few points it would not provide an accurate relationship between intensity and pressure. Ergo, a-priori calibration was utilised instead of in-situ. Of course the advantage of using in-situ calibration is that the intensity ratios obtained during the experiment are not affected by variations in the setup, such as the distance between the model and the camera or between the model and the light source. Also the emitted intensities are already corrected for temperature variations on the model.

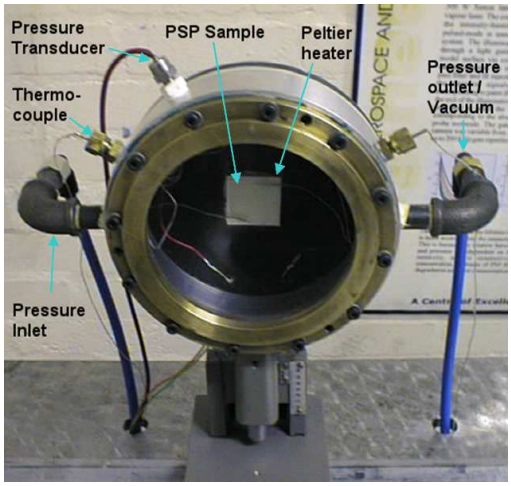

Figure 3: A-priori (static) calibration chamber.

The priori calibration took place in a pressure/temperature controlled chamber shown in figure 3 with the various components outlined [11]. The pressure varied in the range between $0-4$ *bar* and the temperature could be controlled between 270 K to 330 K. The sample was initially illuminated by a pair of LED arrays with peak wavelength of 470 *nm* and then the luminescent emission was captured by a camera (LaVision Imager Intense). A combination of two filters was used to capture the emitted light. The first filter was a long pass filter allowing light with wavelength greater than 600 *nm* to pass, and the second filter was an Infra-Red (IR) cut-off filter, so any light above 700 *nm* would be cut off. The calibration was determined from the ratio between the intensities of the wind-off and wind-on images. The Stern-Volmer coefficients are then used to calibrate the intensity ratios obtained from the experiments.

Figure 4 represents a selection of the raw images obtained from a-priori calibration performed at 294 K at different pressures (the selection is random and is for demonstration purpose only). Figure 5 represents the intensity ratios of the same images when using the first image of figure 4 obtained at 0.5 *bar* as the reference. The intensity of the raw images is not very uniform, this could be due to the non-uniform application of the paint (air brush). The divided images, however, have a much better surface uniformity. This is the reason why in the PSP experiment performed we have taken the ratio of wind-off to wind-on images and applied calibration.

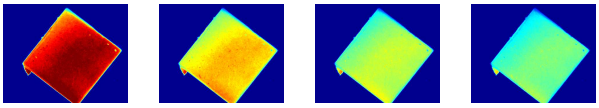

(a) (b) (c) (d)

Figure 4: Raw images obtained from static calibration at pressures: (a) $P = 0.5$ *bar*, (b) $P = 1.3$ *bar*, (c) $P = 1.9$ *bar*, (d) $P = 2.5$ *bar*.

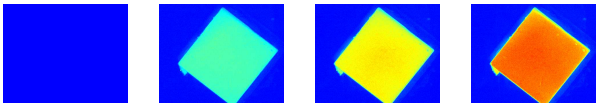

(a) (b) (c) (d)

Figure 5: Results of dividing all the images in figure 4 by figure 4(a), (a) $P = 0.5$ *bar*, (b) $P = 1.3$ *bar*, (c) $P = 1.9$ *bar*, (d) $P = 2.5$ *bar*.

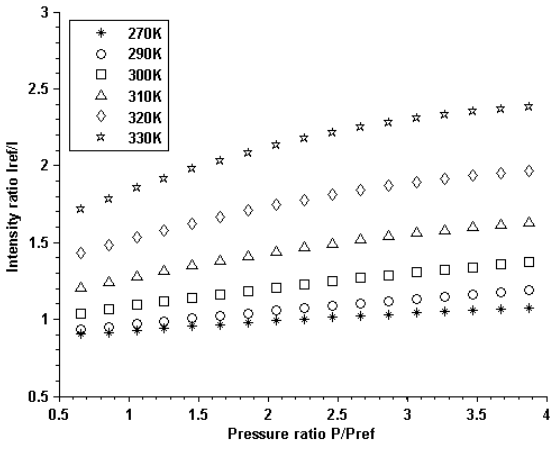

Figure 6: Stern-Volmer plot.

Figure 6 represents the Stern-Volmer plot obtained for various temperatures. The pressure sensitivity of the luminophore was found to increase with increasing temperature. In addition, the high temperature dependence of the paint is a factor that should

be considered during the calibration procedure. By measuring the temperature of the test section the appropriate Stern-Volmer coefficients are determined from a-priori calibration.

The detector Signal to Noise Ratio (SNR) can be improved by summation of a series of images for each run [9].

Steady Flow Through Sonic Nozzle

Figure 7 shows the pressure profile for the two extreme inlet pressures along with the pressures obtained from discrete pressure measurements of the transducers which are in the field of view of the images. The relative error in the PSP measurements is 6.1%. The superiority of the PSP technique in presenting a full quantitative picture of the flow against the discrete pressure measurements is clearly visible in figure 7.

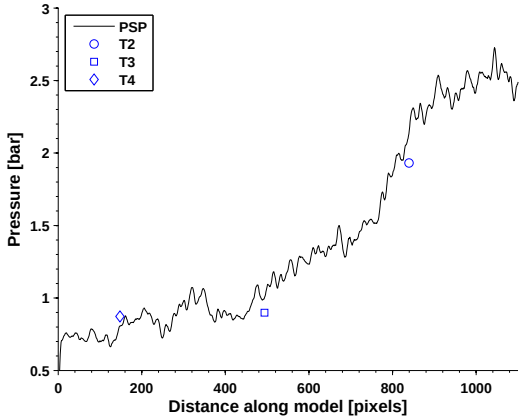

(a)

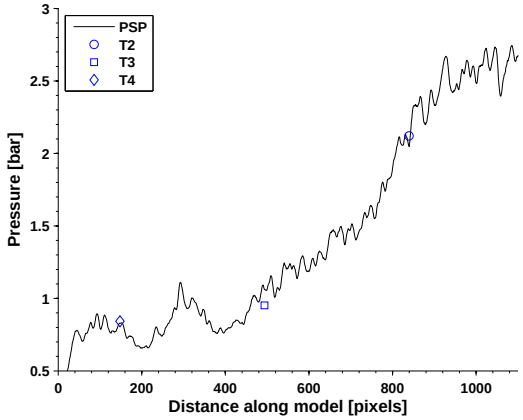

(b)

Figure 7: Comparison between PSP and pressure tappings. a) inlet pressure $P5 = 2.38$ *bar*, b) inlet pressure $P6 = 2.5$ *bar*.

Figure 8(a) and 8(b) show the in-situ calibrated images acquired for two out of the six inlet pressures examined. The profiles of all six inlet pressures, taken along the central axis of the nozzle, shown in figure 8(c). With increase in inlet pressure the static pressure within the converging section also increases. Through the throat of the nozzle, however, the pressure remains almost constant and is not affected by the change in inlet pressure; indicating that the nozzle is choked. Exploring higher pressure, the flow begins to exhibit different characterstics. While the static pressure continued to drop due to the acceleration of the flow through the nozzle, at high pressures the flow appears to be under expanded, hence the flow is capable of additional expansion after leaving the nozzle [1, 3]. This gives rise to the shock structures visible in figure 8(b) in which the pressure at the centreline rises and falls repeatedly [6]. This implies that the flow goes from subsonic to supersonic.

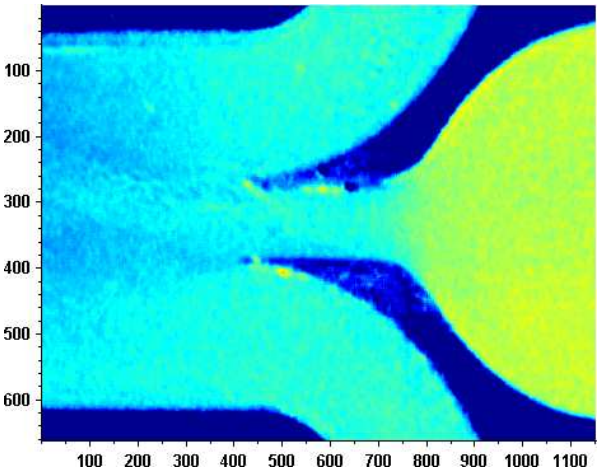

(a)

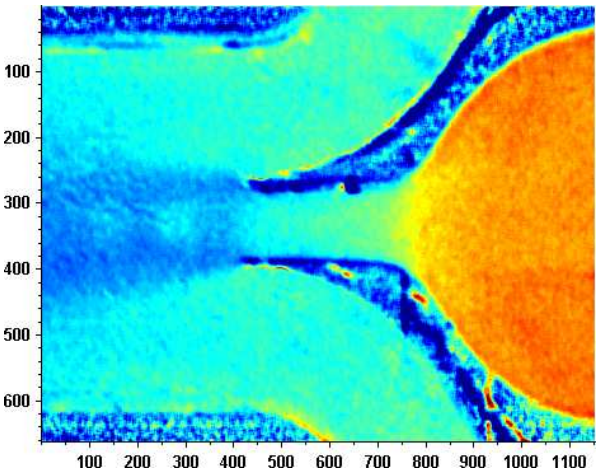

(b)

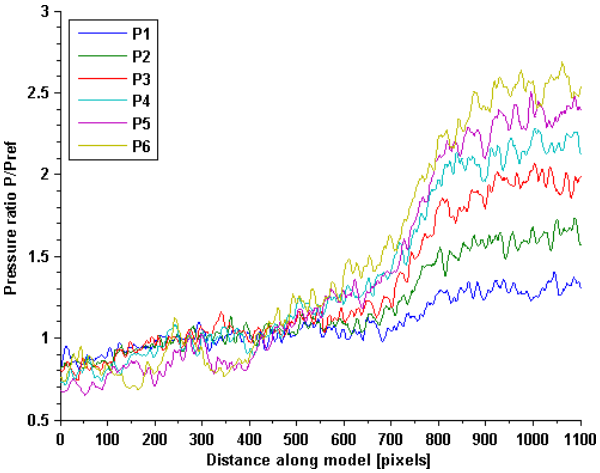

(c)

Figure 8: Pressure map for sonic nozzle, (a) inlet pressure $P = 1.5$ *bar*, (b) inlet pressure $P = 2.5$ *bar*, (c) pressure profiles along the central axis ($y = 330$) for all inlet pressures.

Transonic wind tunnel

Figure 9 presents the schlieren photographs of the flow around the fins, for two of the cases examined; the no dimples case and that of the dimples placed 90^o from the leading edge. Figure 10 shows the PSP results corresponding to the same two cases.

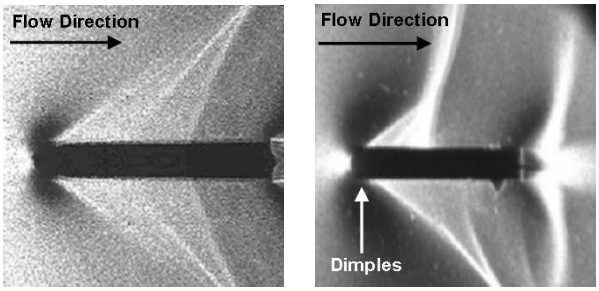

(a) (b)

Figure 9: Schlieren photographs at $M = 0.8$, (a) no dimples, (b) dimples located at 90^o from the leading edge.

For the no dimples case, as shown in figures 9(a) and 10(a), the shock wave system is symmetrical. The dimples affect the local flow field around the leading edge. They induce adverse pressure gradients due to the local surface roughening causing the thickening of the boundary layer. As a result, the dimples alter the effective geometry at the leading edge region. However, due to their location, their effect is not symmetrical. On the upper side (figures 9(b) and 10(b)), a small in size normal shock wave is observed at approximately one-third of the chord-length of the fin.

It is conjectured that the oncoming Mach number (on the upper side) drops quickly, at some distance from the surface, to a value where it is no longer possible to achieve the required pressure jump (flow deflection) across a weak oblique shock wave and the flow downstream turns subsonic. This means that it is not possible for a lambda-shock structure to exist. Presence of the dimples prevents the shock from moving too far downstream, which may lead to reduced shock motion and delay of buffet onset. On the lower section of the wall, an overall decrease of the pressure level is measured, occupying almost the full chord-length of the fin. On the upper section, a strong interaction region is mapped near the apex of the fin corresponding to the location of the normal shock wave.

By taking two profiles, one along the upper and the other along the lower side of the fins, the pressures were compared with that of the transducers located at the same stream-wise location. The results are plotted in figure 11. From the comparisons with the pressure transducer data, and the associated errors related to the calibration procedure, detector noise and effect of illumination non-uniformities, the overall pressure uncertainty in the PSP results was 5%.

Uncertainties in PSP Measurements

The accuracy of intensity-based pressure-sensitive paint optical systems is sensitive to drift and aging of the light source and detector as well as paint in-homogeneities in dye concentration and film thickness. The ratio of wind-off image to wind-on image is processed to eliminate the effects of these factors. However, the effect of the variation of illumination is not cancelled. Aging is another potential source of error but all tests were completed within few hours. Photo-degradation also plays an important role in the accuracy of PSPs. If the paint is exposed to the excitation light for long periods, over time this kills the luminophore molecules causing a reduction in the emitted intensity levels. Because the models used were simple in shape and the aerodynamic loads were small, model deflection was negligible. The accuracy of the technique corresponds to that of the thermocouples and pressure transducers used for calibration, which is in the range of 2.5 K and ± 250 Pa, depending on the absolute temperature and pressure, respectively. Calibration uncertainty also comes from curve fitting the data to equation (1).

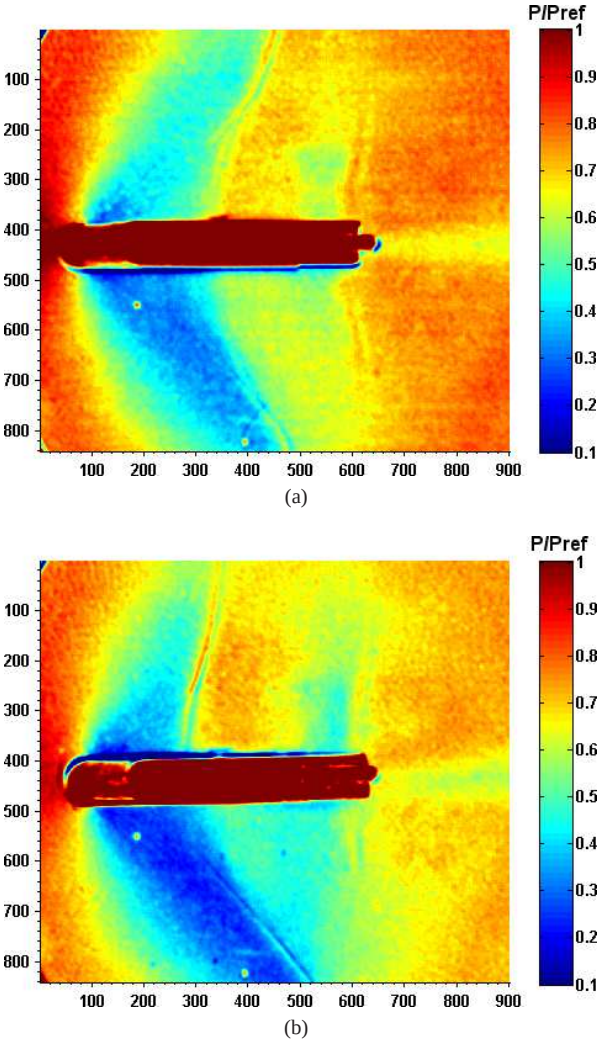

(a)

(b)

Figure 10: PSP images showing pressure distribution at $M = 0.8$, (a) no dimples, (b) dimples located at 90^o from the leading edge on the lower side.

Conclusion

The current study has examined the applicability of a ruthenium based pressure-sensitive paint, to unsteady and high-speed flows. Two test cases have been studied, firstly the flow through a sonic nozzle and secondly the effect of dimples on glancing shock wave turbulent boundary layer interactions at transonic speeds.

The paint has been developed in-house at The University of Manchester by the Aero-Physics Laboratory headed by Dr. K. Kontis. The PSP recipe used has proven not only to provide accurate global pressure measurements but also to pinpoint the physical features of the flow such as the shock structures present, making it a truly molecular image sensing technique for aerodynamic flows.

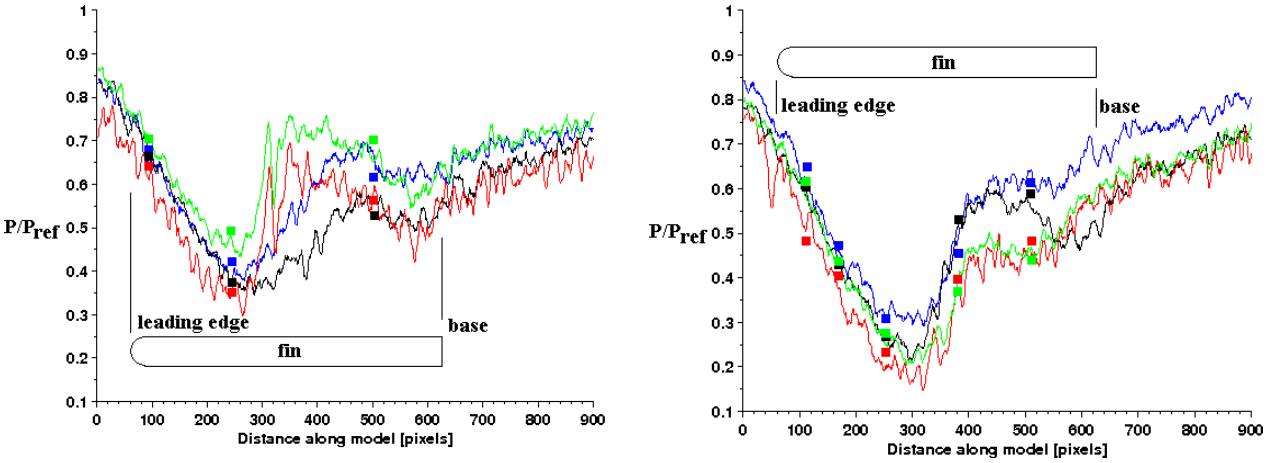

Figure 11: Comparisons in the stream-wise direction of PSP results with discrete measurements of pressure tappings, (a) upper side ($y = 200$), (b) lower side ($y = 640$). —PSP, no-dimples, —PSP, dimples at 0^o, —PSP, dimples at 45^o, —PSP, dimples at 90^o, ■ tapping, no-dimples, ■ tapping, dimples at 0^o, ■ tapping, dimples at 45^o, ■ tapping, dimples at 90^o.

Compared with conventional pressure measurements using transducers, the PSP results presented for the sonic nozzle and the dimples case differed by 6.1% and 5%, respectively.

Currently we are in the process of applying the PSP to more challenging flows such as the hypersonic regime in order to validate the accuracy of the paint and also to examine highly unsteady flows such as moving shock waves.

Acknowledgements

The authors are greatly indebted to Dr. David Ellis from the School of Chemistry and Mr. Robert Glegg from the School of Chemical Engineering and Analytical Science at The University of Manchester for their help and support in the preparation of the PSP. EPSRC support/grant is also acknowledged.

References

[1] Anderson Jr. J.D., *Modern compressible flow with historical perspective*, McGraw-Hill, 1990.

[2] Bjorge S.T., Reeder M.F., Subramanian C., Crafton J. and Fonov S., Flow Around an Object Projected from a Cavity into a Supersonic Freestream, *AIAA Journal*, **73**, 2005, 1465–1475.

[3] Bradley J.J., *Shock Waves In Chemistry And Physics*, Methuen & Co, Ltd, 1962.

[4] Carroll B.F., Abbitt J.D., Lucas E.W. and Morris M.J., Step Response of Pressure-Sensitive Paints, *AIAA Journal*, **34**, 1996f, 521–526.

[5] Lada C., Amir M., Wong C. and Kontis K., Effect of Dimples on Glancing Shock Wave-Turbulent Boundary Layer Interactions, *42nd AIAA Aerospace Sciences Meeting and Exhibit*, 2004, AIAA-2004-1058.

[6] Matsuo K., Miyazato Y. and Kim H.-Y, Shock train and pseudo-shock phenomena in internal gas flows, *Progress in Aerospace Sciences*, **35**, 1999, 33–100.

[7] McLachlan B.G., Bell J.H., Park H., Kennelly R.A., Schreiner J.A., Smith S.C. and Strong J.M., Pressure-Sensitive Paint Measurements on a Supersonic High-Sweep Oblique Wing Model, *Journal of Aircraft*, **32**, 1995, 217–227.

[8] Mosharov V., Radchenko V. and Fonov S., *Luminescent Pressure Sensors in Aerodynamic Experiments*, Central Aerodynamic Institute (TsAGI), Moscow, 1998.

[9] Sakamura Y., Matsumoto M. and Suzuki T., High frame-rate imaging of surface pressure distribution using porous pressure-sensitive paint, *Measurement Science and Technology*, **16**, 2005, 759-765.

[10] Sakaue H., Matsumara S., Schneider S.P. and Sullivan J.P., Anodized Aluminium Pressure Sensitive Paint for Short Duration Testing, *22nd AIAA Ground Testing Conference*, Missouri, 2002, AIAA-2002-2908.

[11] Wong C., Amir M., Lada C. and Kontis K., Molecular image sensing for pressure and temperature surface mapping of aerodynamic flows, *42nd AIAA Aerospace Sciences Meeting and Exhibit*, Reno, 2004, AIAA-2004-598.